Materials Today Communications 29 (2021) 102850

Contents lists available at ScienceDirect

Materials Today Communications

journal homepage: www.elsevier.com/locate/mtcomm

Polystyrene/sepiolites nanocomposite foams: Relationship between composition, particle dispersion, extensional rheology, and cellular structure

A. Ballesteros [a,*], E. Laguna-Gutierrez [b], M.L. Puertas [c], A. Esteban-Cubillo [c], J. Santaren [c], M. A. Rodriguez-Perez [a]

[a] Cellular Materials Laboratory (CellMat), University of Valladolid, Paseo de Belen 7, 47011 Valladolid, Spain
[b] CellMat Technologies S.L., UVA Science Park Building, Paseo de Belen 9-A, 47011 Valladolid, Spain
[c] Tolsa SA, Ctra. Vallecas-Mejorada del Campo (M-203), 28032 Madrid, Spain

ARTICLE INFO

Keywords:
Cellular nanocomposites
Extensional rheology
Sepiolites

ABSTRACT

The main objective of this work is to analyze how the cellular structure of foamed polystyrene based (PS) nanocomposites, produced by gas dissolution foaming, is affected by the extensional rheological behavior of the polymer matrix and by the dispersion degree of the particles. These composites have been produced with different types of natural and organomodified sepiolites and with different contents of these particles. The extensional behavior and the dispersion degree were characterized by extensional and shear dynamic rheology, respectively. The results obtained indicate that the extensional rheological behavior controls the foam degeneration mechanisms; meanwhile, the way in which the particles are dispersed in the PS matrix controls the nucleation mechanisms. Results also indicate that, in these systems, the characteristics of the cellular structure are mainly defined by the way in which nucleation occurs. Therefore, improving the dispersion degree is a key approach to reduce the cell size by 90%, with respect to the pure polymer.

1. Introduction

One procedure to improve the thermal and also the electrical and mechanical properties of foams consists of incorporating nanoparticles into the polymer matrix [1–3]. These foams, produced from polymer nanocomposites, are known as cellular nanocomposites. These materials combine the advantages of having a cellular structure with the beneficial effects provided by the nanoparticles [4]. Nanoparticles act in two different ways. On the one hand, nanoparticles can modify the characteristics of the cellular structure, and, on the other hand, nanoparticles can improve the morphology and properties of the solid polymer matrix present in the cell walls. A small amount of well-dispersed nanoparticles will act as nucleation sites modifying the cellular structure and leading to lower cell sizes and higher cell nucleation densities [5]. Nanoparticles can also modify the extensional rheological properties of the polymer matrix, which have an important effect on the degeneration mechanisms and, as a consequence, on the cell size, cellular structure homogeneity and foam density [6–8].

Polystyrene (PS) has been selected for this work because the foams based on this polymer are the most used in the foam market, after polyurethane (PU) foams. They are commonly employed as thermal insulators thanks to their low thermal conductivity [9,10].

It is well known that the thermal conductivity strongly depends on some parameters of the cellular structure such as cell size or porosity [11]. The incorporation of nanoparticles is an interesting strategy to improve the thermal properties of the foams in a significant way, by modifying the characteristics of the cellular structure [12]. The effects of incorporating nanoparticles into a PS matrix, intended for foaming applications, have been evaluated in previous works. Zhang et al. showed that the introduction of activated carbon (AC) nanoparticles makes it possible to improve the thermal insulation performance of PS foams [12]. Han et al. showed that the inclusion of nanoclays in a PS matrix leads to a reduction of the cell size and to an increase of the cell density. Moreover, the cellular nanocomposites exhibited higher tensile modulus, improved fire retardance, and better barrier properties [13]. Fei et al. demonstrated that the inclusion of lignin into PS in contents between 10 wt% and 50 wt% helped to control the cell size and cell density of the foamed samples and also increased their maximum sound

* Corresponding author.
E-mail address: albalag@fmc.uva.es (A. Ballesteros).

https://doi.org/10.1016/j.mtcomm.2021.102850
Received 4 July 2021; Received in revised form 19 September 2021; Accepted 27 September 2021
Available online 29 September 2021
2352-4928/© 2021 The Authors. Published by Elsevier Ltd. This is an open access article under the CC BY-NC-ND license (http://creativecommons.org/licenses/by-nc-nd/4.0/).

absorption coefficient, at normal incidence, in values higher than 0.9 [14]. Finally, Shen et al. claimed that the use of carbon nanofibers in PS foams created a protective layer around the cell walls that resulted in the enhancement of the foam strength [15].

Most of the works dealing with nanoparticles are based on the use of spherical or layered particles [13]. Particles like montmorillonites, silica or nano-porous silica have been extensively used for the production of cellular PS based composites [16–18]. However, it is not easy to find in literature studies analyzing the effects that needle-like shape particles, like sepiolites, could have on the final cellular structure of PS foams [19–24]. In fact, there is not plenty of literature that studies the use of sepiolites to modify the cellular structure of PS foams. The only publication we have detected on this topic is the one performed by Notario et al. [25] The authors reported that it is possible to reduce the cell size of PS foams by 60% just by adding 0.5 wt% of sepiolites. However, this work does not report an exhaustive and systematic study of how the dispersion degree of these particles as well as the extensional rheological behavior of the solid polymer composite affect the cellular structure of the foams.

Sepiolites are natural clays with a needle-like shape, with thicknesses in the nanometric scale, between 10 and 12 nm, large surfaces areas ca. 300 m^2/g, densities close to 2.1 g/cm^3 and high aspect ratios. The structure of sepiolites consists of blocks of two tetrahedral silica sheets sandwiching an octahedral sheet of magnesium oxide hydroxide. The dimensions of the cross-section tunnels are about 0.36 nm x 1.1 nm. The discontinuity of the silica sheets allows the presence of a significant number of silanol (Si-OH) groups on the surface of the particles. These silanol groups can enhance the interfacial interaction between the nanoparticles and the polymer and therefore, improve the dispersion of sepiolites in the polymeric matrix. These properties make sepiolites suitable for being properly dispersed in different kinds of polymers. Bernardo et al. have analyzed the role of sepiolites as nucleating agents in a polymethyl methacrylate (PMMA) matrix. They found that it was possible to decrease the cell size by a factor of 5 by incorporating 1.5% of sepiolites [19]. Furthermore, sepiolites can also have a decisive influence on some properties of the polymer matrix like in the flammability behavior, mechanical or thermal properties. For instance, sepiolites could work as fire- retardant agents in polymers when they are combined with other additives like decabromodiphenyl ether (DBDPE) or antimony trioxide (ATO) [26]. Huang et al. reported that sepiolites have a synergetic effect with some intumescent flame retardant agents and that they could improve the performance of a material based on polypropylene (PP) thanks to the barrier effect that they produce and the capability of these particles to increase the char residue formation [27]. Mechanical properties are also modified by the inclusion of sepiolites [28]. In particular, Zheng et al. proved that by incorporating 1 wt% of sepiolites in epoxy nanocomposites it was possible to double the flexural strength and multiplying by a factor 5 the impact strength [29]. Finally, thermal properties, like thermal stability, are also altered when sepiolites are incorporated into the polymer matrix [30,31]. Garcia-Lopez et al. show that by incorporating 6% of sepiolites to a polyamide 6, it was possible to increase the heat deflection temperature up to 2.5 times, compared to the one of the pure polymer [32].

All these improvements in the structure and properties of solid polymers induced by sepiolites are interesting; however, in the case of polymeric foams, these properties are conditioned by the way in which the extensional rheological behavior of the polymer matrix is modified by the incorporation of these particles and by the way in which the particles are dispersed in the polymer matrix. To produce foams with high expansion ratios and homogeneous cellular structures with low cell sizes it is necessary that the extensional viscosity of the polymer matrix increases as the polymer is elongated, due to the extensional forces occurring during the foaming process [33,34]. In the initial moments of cell growth, it is desired that viscosity takes low values to permit bubbles to grow. Later, as the polymer is stretched due to the cell growth, a high extensional viscosity is required. This way, the polymer matrix can resist the foam expansion without breaking. This behavior, that is, this abrupt increase of extensional viscosity as time or strain increases is usually known as strain hardening [35–37]. The aforementioned effect has remarkable importance in helping cell walls to withstand the deformation during the last stages of the foaming process and therefore, to reduce the degeneration mechanisms (coalescence, drainage and coarsening) [38]. Some authors have investigated the influence of nanoparticles in the uniaxial extensional flow with diverse results. A considerable number of authors have reported and alignment of the nanoparticles in the uniaxial extensional flow, increasing the melt strength of the polymers or inducing strain hardening to the melt [39–41]. Contrary to this theory, Okamoto et al. declared that the strain hardening is a result of the perpendicular disposition of particles to the direction of the force [8]. The effect of the clay content on the strain hardening has also been analyzed. Kotsilkova et al. observed an increase in the strain hardening in PMMA with the inclusion of high contents of smectite particles (between 10% and 15%) [42]. Nevertheless, Gupta et al. mentioned that the presence of silicate layers (contents of bentonite between 2.5% and 5%) in ethylene-vinyl acetate (EVA) might induce solid-like behavior and increase the extensional viscosity, compared to the unfilled material, due to the reorganization of the clay layers during the extensional process [43]. However, this increase in the extensional viscosity takes part until a certain value of the Hencky strain, beyond this point the contribution of the polymer chains dominates over the contribution of the particles. Finally, Laguna-Gutierrez et al. reported that on some occasions the strain hardening could be strongly decreased by the presence of particles [39]. This is a behavior that several authors have also reported [44–47]. They have considered that particles can interfere with the occurrence of the strain hardening phenomenon since they are partially converting the extensional flow in the surrounding polymer into shear flow.

On the other hand, it is also crucial to understand how the dispersion degree of the particles in the polymer matrix affects the final properties of the foamed sample. The relation between the dispersion of the particles and the nucleation process during the foaming step is remarkable [4]. The nucleation mechanisms can be modified and controlled by the inclusion of particles which can work as heterogeneous nucleation sites in which the energy nucleation barrier, defined as the minimum energy necessary to start the nucleation process, is reduced [48]. However, only when the dispersion degree of the particles in the polymer matrix is optimal, it is possible to increase the cell density and reduce the cell diameter, compared to the virgin material [49]. Furthermore, the final properties of the foamed samples are affected by the characteristics of the cellular structure, which, in turn, are conditioned by the dispersion degree [50]. As a consequence, plenty of strategies have been proposed to accomplish a good dispersion of the fillers, among others: ultra-sonication of particles, high shear mixing processes or the functionalization of the particles [32,50–52].

An excellent dispersion of particles over the polymer and hence, a god nucleating effect can be achieved. However, if particles modify the extensional behavior of the material in the wrong way (that is, particles lead to a reduction of the polymer strain hardening), the degeneration phenomena would appear, and the improvements obtained in the cellular structure could be lost. Therefore, the main objective of this work is to analyze how the extensional rheological behavior of the PS matrix is affected by the incorporation of sepiolites as well as to understand the relationships between extensional rheology, dispersion degree and cellular structure. This new knowledge will allow determining which of these two parameters (extensional behavior or dispersion) has more influence when it comes to achieving an optimum cellular structure and will provide the opportunity of having a more exhaustive control over the foaming process and therefore, about the structure and properties of foamed nanocomposites based on PS and sepiolites.

Table 1
Summary of the formulations produced during the present study.

Sample Name	*Content of Polymer (wt%)*	*Content of Sepiolites (wt%)*	*Content of Antioxidant (wt%)*
PURE PS	99.5	0.0	0.5
PS + 2% N-SEP	97.5	2.0	0.5
PS + 2% O-QASEP	97.5	2.0	0.5
PS + 2% O-SGSEP	97.5	2.0	0.5
PS + 6% N-SEP	93.5	6.0	0.5
PS + 6% O-QASEP	93.5	6.0	0.5
PS + 6% O-SGSEP	93.5	6.0	0.5
PS + 8% N-SEP	91.5	8.0	0.5
PS + 8% O-QASEP	91.5	8.0	0.5
PS + 8% O-SGSEP	91.5	8.0	0.5
PS + 10% N-SEP	89.5	10.0	0.5
PS + 10% O-QASEP	89.5	10.0	0.5
PS + 10% O-SGSEP	89.5	10.0	0.5

2. Experimental

2.1. Materials

A commercial PS recommended for foam applications (INEOS, Styrolution PS153F) with a melt flow index of 7.5 g/10 min (200 ºC/5 kg) and a glass transition temperature (T_g) of 102 ºC was used as polymer matrix. Three kinds of sepiolites kindly supplied by Tolsa S.A. (Madrid, Spain) were used in this work: natural sepiolites (N-SEP), sepiolites organically modified with quaternary ammonium salts (O-QASEP) and sepiolites organically modified with silanol groups (O-SGSEP). The wet milling process and the organo-modification of the particles were reported in a previous work [53].

An antioxidant (BASF, Irganox 1010) is also used to avoid thermal degradation during the extrusion stage. Finally, a medical-grade carbon dioxide (CO_2) (99.9% purity) was used as a blowing agent for the gas dissolution foaming experiments.

2.2. Production process

Before materials were processed, they were dried in a vacuum drying oven (Mod. VacioTem TV, P-Selecta) at 70 ºC for 4 h, in the case of pure PS, and at 80 ºC for 8 h, in the case of the different types of sepiolites. The mixing of the polymer with the sepiolites was carried out in a twin-screw extruder (Collin ZK 25 T with L/D of 24) using a temperature profile that goes from 145 ºC to 185 ºC (at the die of the extruder) and with a screw rate of 50 rpm. The different formulations produced in this study are shown in Table 1. Formulations containing 0 wt%, 2 wt%, 6 wt%, 8 wt% and 10 wt% of sepiolites were produced.

The different nanocomposites were then thermoformed in a hot plate press to obtain materials with the desired shape and size. The compression molding process was performed at a temperature of 235 ºC and at a pressure of 27 bars. Samples with different dimensions were produced for the different tests. Rectangular prisms with the following dimensions: 20 × 10×0.5 (L x W x T) mm were produced for the extensional rheological characterization. Moreover, cylindrical samples with a radius of 11 mm and a thickness of 2 mm were produced to perform the shear dynamic measurements. Finally, samples with diameters of 150 mm and thicknesses of 2 mm were also produced by compression molding. From these samples different specimens with the following dimensions: 20 × 20×2 (L x W x T) mm were obtained for the foaming tests.

2.3. Foaming process

The foaming of the samples was carried out using the solid-state gas dissolution foaming method [54]. For this purpose, a high-pressure vessel, PARR 4681 from Parr Instrument Company, with a capacity of 1 l and capable of operating at a maximum temperature of 350 ºC and at a maximum pressure of 41 MPa, was used. This reactor is equipped with a pressure pump controller, SFT- 10 from Supercritical Fluid Technologies Inc., which is controlled automatically to keep a constant pressure. The pressure vessel is also equipped with a clamp heater of 1500 W where the temperature is controlled via a temperature controller (CAL 3300 from CAL controls). The previously mentioned solid-state gas dissolution foaming process consists of two steps [55]. Samples were firstly introduced in the pressure vessel at 8 MPa of CO_2 pressure for the saturation stage. The saturation temperature was 40 ºC and the saturation time was 24 h. It was proved that these conditions are enough to achieve full saturation of CO_2 in the PS based materials. After saturation, the pressure was abruptly released. Finally, for the foaming stage, samples were removed from the pressure vessel and introduced in a thermostatic silicon bath at 120 ºC for 1 min. The time between the release of the pressure and the immersion in the thermal bath was 2 min. Once the materials have expanded, they were cooled in water to stabilize the cellular structure.

2.4. Characterization

2.4.1. Extensional rheology

A stress-controlled rheometer (AR 2000 EX from TA Instruments) with an extensional fixture (SER 2, Xpansion Instruments) was used to analyze the extensional rheological behavior of the different solid, non-foamed, composites. In this device, the samples are clamped to two cylinders that rotate, at a fixed rate, in opposite directions applying a uniaxial stretching force to the material. All the experiments were conducted at a temperature of 160 ºC and at different Hencky strain rates: 0.3, 0.5 and 1 s^{-1}. In all the experiments the maximum Hencky strain was 2.8. Extensional viscosity can be defined as the ratio between the measured stress and the corresponding Hencky strain rate. A more detailed description of the measurement protocol can be found elsewhere [39].

From the extensional viscosity measurements, the strain hardening coefficient (S) was obtained. This parameter (see Eq. 1), which allows quantifying the way in which the extensional viscosity increases when time or strain increases, has been obtained for the different formulations.

$$S = \eta_E^+(t, \dot{\varepsilon_0})/\eta_{E0}^+(t) \quad (1)$$

Where $(\eta_E^+(t, \dot{\varepsilon_0}))$ is the transient extensional viscosity for a determined time (t) and Hencky strain rate ($\dot{\varepsilon_0}$) and $\eta_{E0}^+(t)$ is the transient extensional viscosity in the linear viscoelastic regime, which can be obtained in two different ways: as three times the time-dependent shear viscosity growth curve at very low shear rates or by extrapolating the overlapping parts of the extensional curves at different elongation rates [56]. In the present work, the second option was chosen to obtain the strain hardening coefficient. This coefficient has been determined for a time of 2.67 s and for a Hencky strain rate of 1 s^{-1}.

2.4.2. Shear rheology

A shear stress-controlled rheometer (AR 2000 EX from TA Instruments) was used to measure the dispersion degree of the different solid, non-foamed, formulations. Dynamic shear measurements were conducted at a temperature of 220 ºC under a nitrogen atmosphere using

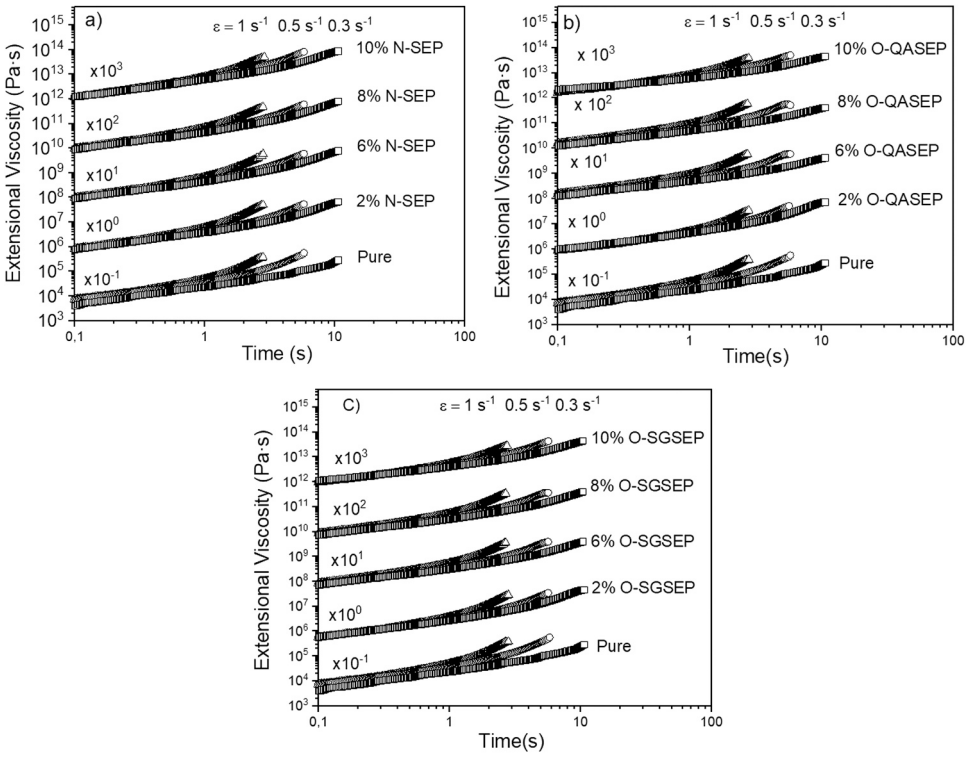

Fig. 1. Extensional viscosity behavior of the composites containing different amounts of particles. a) PS based composites containing different contents of N-SEP. b) PS based composites containing different contents of O-QASEP. c) PS based composites containing different contents of O-SGSEP.

25 mm diameter parallel plates. A fixed gap of 1 mm was selected to perform the rheological measurements.

The first step was to perform a strain sweep test at a fixed dynamic frequency (1 rad s^{-1}) to determine the linear viscoelastic regime of the different nanocomposites. Then, a time sweep was performed to recover the initial state of the particle network that was partially deformed when the sample was loaded in the rheometer. The duration of the time sweep varied between 360 s and 600 s, depending on the material. Finally, the frequency sweep step was performed, in a range of angular frequencies varying between 0.01 rad s^{-1} and 100 rad s^{-1}. From these measurements, four properties were analyzed: dynamic shear viscosity ($|\eta^*|$), storage modulus ($(G'(\omega))$), loss modulus ($(G''(\omega))$) and crossover frequency (ω_x).

2.4.3. Gas uptake

The method used during the present work to measure the gas absorbed by the polymer matrix, during the saturation stage, was the gravimetric method. By using this method, the gas uptake (CO_2 Uptake) was obtained directly by determining the weight gained by the polymer sample during the sorption stage. This parameter was determined according to Eq. (2).

$$CO_2 \text{ Uptake} = \left(W_s - W_0\right)/W_0 \quad (2)$$

Where W_s is the weight of the polymer composite after the saturation stage, when the polymer matrix is fully saturated, and W_0 is the initial weight of the sample before being introduced in the pressure vessel. The time between the depressurization of the pressure vessel and the weight of the sample was around 2 min. These measurements are only an estimation of the solubility and they have been used to establish a comparison between the behavior of the different samples.

2.4.4. Density

The density of the solid materials was analyzed using a gas pycnometer (Accupyc II 1340 from Micromeritics). The density of the foamed materials was determined by the geometric method, that is, dividing the corresponding mass of each specimen by its geometric volume (ASTM standard D1622–08).

The following equations (Eqs. 3 and 4) show the way of determining the relative density and expansion ratio. Relative density (ρ_r) is defined as the ratio between the density of the foam (ρ_{foam}) and the density of the bulk solid material (ρ_{solid}). On the other hand, the expansion ratio (E) is defined as the inverse of the relative density (ρ_r).

$$\rho_r = \rho_{foam}/\rho_{solid} \quad (3)$$

$$E = 1/\rho_r \quad (4)$$

2.4.5. Open cell content

To evaluate the open cell content (OC) of the different foamed samples, according to the Standard ASTM D6226–10, a gas pycnometer, Accupyc II 1340 from Micromeritics, was used. To obtain the open cell content Eq. (5) was employed.

$$OC(\%) = 100\left(v_{geometric} - v_{pycnometer}/V_{geometric} \quad p\right) \quad (5)$$

Where $v_{geometric}$ is the geometric volume of the sample, $v_{pycnometer}$ is the volume of the sample obtained with the pycnometer and p is the porosity calculated as $(1 - \rho_{foam}/\rho_{solid})$, where ρ_{foam} is the density of the foam and ρ_{solid} is the density of the solid matrix.

2.4.6. Structural characterization

The structure of the cellular materials was analyzed with a scanning electron microscope (SEM) (Jeol, Mod. JSM-820). Parameters such as the average cell size (Φ), the cell nucleation density (N_0), the relative volume fraction occupied by the small cells (v_s) and the homogeneity of the cellular structure (SD/Φ) were analyzed with an image processing tool based on the software Fiji/Image J [57]. More than 100 cells of different regions of each cellular material have been analyzed to determine these parameters.

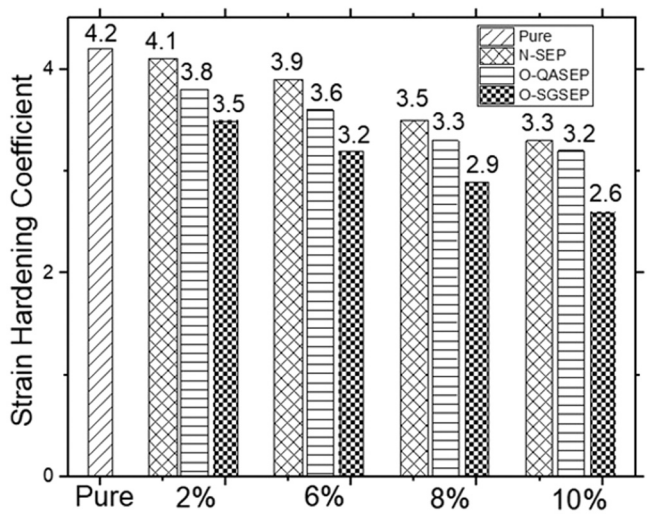

Fig. 2. Strain hardening coefficient obtained for the pure PS and for the composites containing different contents of N-SEP, O-QASEP and O-SGSEP. This parameter has been determined for a time of 2.67 s and for a Hencky strain rate of 1 s^{-1}.

The average cell size is defined as it is indicated in Eq. (6):

$$\phi = \sum_{i=1}^{n} \phi_i / n = \sum_{i=1}^{n} cf/2n(\phi_x^i + \phi_y^i) \quad (6)$$

Where n is the total number of cells counted in the image, ϕ_i is the three-dimensional value of the cell size for and specific cell. ϕ_x^i, ϕ_y^i, are the length of the cells in the directions x and y, respectively, and cf is a correction factor used to correct the two-dimensional value of the cell size to a three-dimensional value of this parameter. As it was indicated in the work of Pinto et al. a value of 1.273 has been selected for the mentioned correction factor [57].

The cell nucleation density (N_0), defined as the number of cells per unit volume of the solid, was obtained using the Kumar's theoretical approximation as it is indicated in Eq. (7) [55]. In this formula N_v is the cell density, defined as the number of cells per cubic centimeter of the foamed material, and ρ_r is the relative density.

$$N_0 = N_v/\rho_r \quad (7)$$

In this work, the cellular materials containing sepiolites present a bimodal structure: small cells, combined with large cells (cells that present sizes higher than 200 μm). Even though the number of large cells is quite low compared to the one of the small cells, the volume that the large cells occupy it is not negligible. For this reason, to quantify the observed bimodality the relative volume fraction occupied by the large cells (v_l) is defined as it is indicated in Eq. (8):

$$v_l = 1 - 100(A_t - A_l/A_t) \quad (8)$$

Where A_l is the area occupied by the large cells in the SEM images and A_t is the total area of the image. In the pure PS foams, which do not present a bimodal structure, this parameter was not calculated, and it is considered as zero.

Finally, the ratio between the standard deviation of the cell size distribution (SD) and the average value of the cell size (SD/Φ) allows analyzing the homogeneity of the cellular structure. Low values of this parameter are related with an homogeneous cellular structure with a narrow cell size distribution.

3. Results

3.1. Extensional rheology

In this section, the effects on the extensional viscosity produced by changing the type and the percentage of sepiolites are evaluated.

Fig. 1 shows the values of the transient extensional viscosity as a function of time for the virgin PS and for the composites containing 2 wt %, 6 wt%, 8 wt% and 10 wt% of N-SEP, O-QASEP and O-SGSEP. Curves

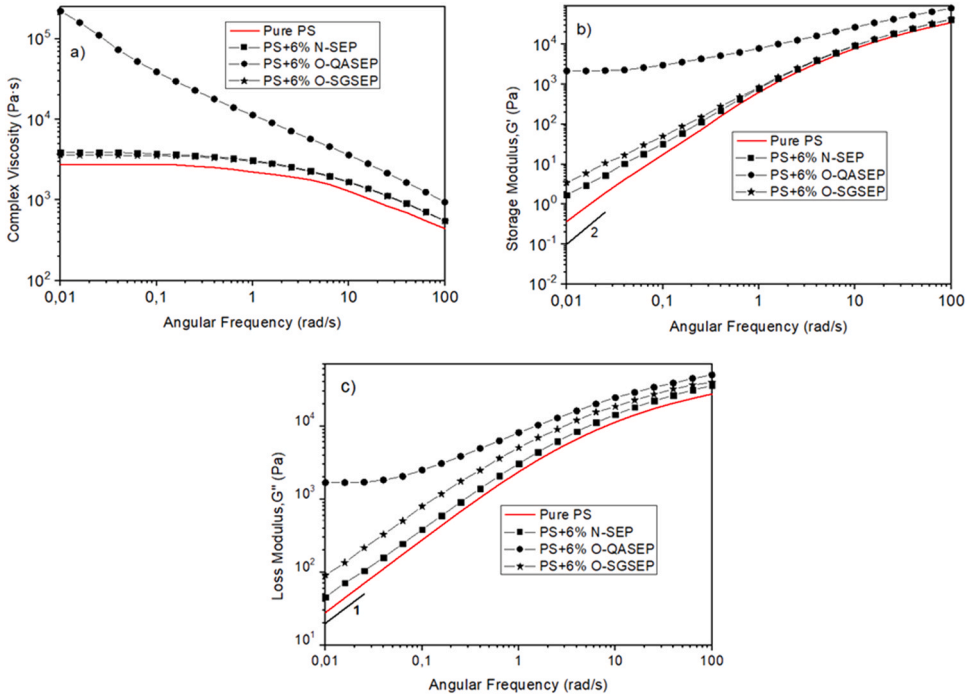

Fig. 3. Viscoelastic properties of the pure PS and the different composites produced with a fixed content of sepiolites (6 wt%). (a) Complex viscosity vs. angular frequency. (b) Storage modulus vs. angular frequency. (c) Loss modulus vs. angular frequency. Common slopes values for a pure polymer are also shown in Fig. 3(b) and (c).

have been multiplied by a factor (included in the figure) to make possible the comparison of the different materials in a single figure.

Results indicate that all the formulations exhibit strain hardening. It is possible to appreciate slight differences in the way in which strain hardening occurs depending on the type of particles employed. The pure PS and the formulation containing N-SEP present a more abrupt strain hardening than that presented by the formulations containing treated particles (O-QASEP and O-SGSEP). Furthermore, the obtained results indicate that the strain hardening of the polymer composites is always lower than the strain hardening of the pure PS. This phenomenon is especially remarkable for the formulations with high percentages of sepiolites (10 wt%). In order to quantify this behavior and evaluate how the strain hardening changes as the content of particles increases, the strain hardening coefficient of the different formulations has been quantified using Eq. (1) and the obtained results are depicted in Fig. 2.

Fig. 2 shows the value of the strain hardening coefficient of the different formulations. As it was previously indicated, this coefficient has been determined for a time of 2.67 s and for a Hencky strain rate of 1 s^{-1}. The pure PS presents the highest strain hardening coefficient (value of 4.2). The incorporation of sepiolites leads to a reduction of the strain hardening coefficient, independently of the type of particles employed. However, the magnitude in which the strain hardening decreases depends on the type of particles. The strain hardening of the formulations produced with the O-QASEP and with the O-SGSEP is always lower than the strain hardening of the formulations produced with the N-SEP, being the strain hardening of the composites produced with the O-SGSEP the lowest one. For instance, at the same percentage of particles, 6 wt%, for example, when adding N-SEP a reduction of the strain hardening close to 7%, with respect to that of pure PS, is detected. When adding the same amount of O-QASEP and O-SGSEP the reduction increases up to 14.0% and up to 22.0%, respectively.

Considering the results obtained in the literature, there are several theories to explain the results obtained in this work. The reduction detected in the strain hardening as the clay content increases could be explained considering that this kind of needle-like shape nanoparticles cannot be aligned in the uniaxial extensional flow direction [16,42]. Another theory is that based on the work of Gupta et al. [28] They indicated that the polymeric composites behave like solid-like materials when their structures are percolated or close to percolation. In this state, they detected a decrease of the strain hardening under uniaxial extensional forces. In the present study a remarkable decrease in the strain hardening occurs when the clay content increases. It is important to remark that the formation of a percolated network structure becomes favored when particles with a large aspect ratio, like sepiolites, are introduced in the system. When this percolated network is obtained the properties of the composite are notoriously affected. Other works proposed that the introduction of particles partially converts the extensional flow in the surrounding polymer into a shear flow. As a consequence, the strain hardening can be strongly decreased by the presence of particles [45–48,58].

3.2. Shear rheology

The dispersion degree of the particles in the polymer matrix has been analyzed by means of shear dynamic rheology measurements considering the formulations containing 6 wt% of particles.

Fig. 3 shows the behavior of the complex viscosity ($|\eta^*|$) (Fig. 3(a)), the storage modulus ($G'(\omega)$) (Fig. 3(b)), and loss modulus ($G''(\omega)$) (Fig. 3(c)) as a function of the angular frequency for the pure PS matrix and the three types of composites under study. Fig. 3(a) shows that the composites present a higher viscosity than the pure PS matrix. This increment is chiefly remarkable for the formulation containing O-QASEP. Moreover, in this composite the Newtonian behavior observed at low frequencies in the other materials disappears and the behavior corresponds to that of a non-Newtonian power-law material.

Table 2
Linear viscoelastic properties of the pure PS and the different composites containing a 6 wt% of different types of sepiolites.

Sample Name	*Zero-Shear Viscosity, η_0 (Pa·s)*	*Slope of G' (Pa·s)*	*Slope of G'' (Pa·s)*	*Crossover Frequency, ω_x (rad/s)*
PURE PS	2905	1.78	0.96	42.29
PS + 6% N-SEP	3839	1.27	0.95	41.18
PS + 6% O-QASEP	Non-Newtonian	0.67	0.75	3.67/28.67
PS + 6% O-SGSEP	3498	1.32	0.92	42.16

For the materials presenting a Newtonian plateau, the zero-shear viscosity (η_0) has been obtained as the value of the viscosity in the Newtonian plateau. The results of zero-shear viscosity are collected in Table 2.

Storage modulus ($G'(\omega)$) is altered by variations in the molecular structure of polymers. At low frequencies, in the area known as terminal region, where the longest relaxation times play a major role, the storage modulus of pure polymers is proportional to the square of the frequency $G' \propto \omega^2$ [58]. In other words, for a pure polymer it is expected that the slope of G' presents a value close to 2. To quantify the changes in the storage modulus, caused by the incorporation of particles, the slopes of the G' curves in the terminal region (between 0.01 and 0.1 rad s^{-1}) were measured. The obtained results are collected in Table 2. As soon as the density of particles per unit volume increases, the values of the slope should approach to 1. When the formulations reach a percolation state, the slope of G' should present values close to 0 [60]. It is important to mention that the density of particles could increase due to two main reasons: an increase in the percentage of particles introduced in the polymeric matrix or in the case of a fixed content of particles, like in this case, an increase of the dispersion degree of the particles in the polymer matrix. Fig. 3(b) shows the differences between the curves of the formulations that contain particles and that of the pure polymer. The slopes of the curves in the terminal region are clearly reduced in the systems containing particles. A reduction of 28% of the slope of G' is achieved when adding 6 wt% of N-SEP. Meanwhile, a decrease of the slope of 62% and 26% is obtained when adding 6 wt% of O-QASEP and 6% of O-SGSEP, respectively. Furthermore, as it is indicated in Table 2, the slope of G' corresponding to the composite containing 6 wt% of O-QASEP particles presents a value close to 0, which indicates that these particles are better dispersed than the others.

On the other hand, the loss modulus, $G''(\omega)$ of a pure polymer should be proportional to the frequency in the terminal region $G'' \propto \omega$ [58]. In other words, for a pure polymer it is expected that the slope of G'' presents a value close to 1. The effect of the type of particles in the loss modulus is shown in Fig. 3(c). The slopes of G'' in the terminal region have been also calculated and the values obtained are shown in Table 2. The slopes of G'' for the systems containing N-SEP and O-SGSEP are similar to that of the pure polymer. On the other hand, the slope of the composite containing O-QASEP is lower. A reduction of 21% is reported, which once again indicates a much better dispersion of this type of particles in the PS matrix. The crossover frequency (ω_x) has been also measured (see Table 2). This parameter is defined as the frequency at which the storage modulus $G'(\omega)$ and the loss modulus $G''(\omega)$ intersect. The presence of one single crossover point indicates that material is not already percolated [59]. On the other hand, the presence of two crossover points indicates that the density of particles is close to the percolation threshold. Finally, a spectrum in which no crossover points appear implies that the density of particles is higher than the percolation threshold [59]. Results indicate that the composites produced with 6 wt % of N-SEP and with 6 wt% of O-SGSEP only show a single crossover point, which means that in these materials a network structure has not

Table 3
Gas uptake during the sorption process, relative density and expansion ratio of the cellular materials produced by gas dissolution foaming.

Sample Name	*Gas Uptake (%wt.)*	*Relative Density*	*Expansion Ratio*
Pure PS	7.69 ± 0.18	0.031 ± 0.007	31.92 ± 1.06
PS + 2% N-SEP	7.86 ± 0.24	0.030 ± 0.008	33.00 ± 0.82
PS + 2% O-QASEP	7.93 ± 0.39	0.027 ± 0.004	35.83 ± 0.93
PS + 2% O-SGSEP	7.90 ± 0.16	0.029 ± 0.001	34.36 ± 1.06
PS + 6% N-SEP	8.19 ± 0.38	0.030 ± 0.006	33.00 ± 1.21
PS + 6% O-QASEP	8.22 ± 0.48	0.030 ± 0.002	33.24 ± 0.77
PS + 6% O-SGSEP	8.15 ± 0.76	0.031 ± 0.004	32.08 ± 1.04
PS + 8% N-SEP	8.34 ± 0.18	0.031 ± 0.005	31.46 ± 1.31
PS + 8% O-QASEP	8.38 ± 0.26	0.030 ± 0.007	32.66 ± 0.96
PS + 8% O-SGSEP	8.18 ± 0.49	0.033 ± 0.006	30.02 ± 0.66
PS + 10% N-SEP	8.13 ± 0.55	0.033 ± 0.001	29.46 ± 0.58
PS + 10% O-QASEP	8.25 ± 0.58	0.032 ± 0.002	30.76 ± 1.01
PS + 10% O-SGSEP	8.03 ± 0.16	0.035 ± 0.006	28.36 ± 0.79

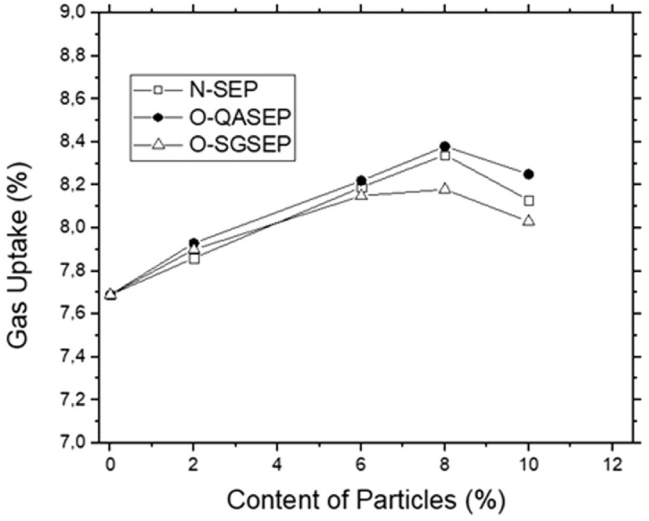

Fig. 4. Percentage of gas uptake as a function of the content of particles.

been formed. Meanwhile, for the material produced with 6 wt% of O-QASEP two crossover points have been obtained, which indicates that this composite presents a percolated structure.

The rheological results indicate that O-QASEP presents a much better dispersion degree than the other two particles. On the other hand, the formulations containing O-SGSEP and N-SEP exhibit a rheological behavior very similar to that of the pure PS matrix, which indicates a poor dispersion of the particles in the polymer matrix.

3.3. Gas uptake and foam density

This section analyzes how the incorporation of sepiolites affects the gas uptake by the polymer matrix as well as the density, and cellular structure of the foamed materials produced gas dissolution foaming. Moreover, the obtained results are related with those obtained after the analysis of both extensional and shear rheological properties.

The results obtained for gas uptake, relative density, and expansion ratio are collected in Table 3.

Fig. 4 shows the effect of the content of particles on the gas uptake. The different formulations present a similar behavior independently of the type of particles employed (with or without surface treatment). An increase of the gas uptake is detected when the amount of sepiolites increases up to values close to the 8 wt%. This result indicates that due to the incorporation of sepiolites the material can absorb more gas (CO_2). The explanation of this behavior could be that sepiolites are CO_2-philic particles. This type of trend has been detected in other systems.

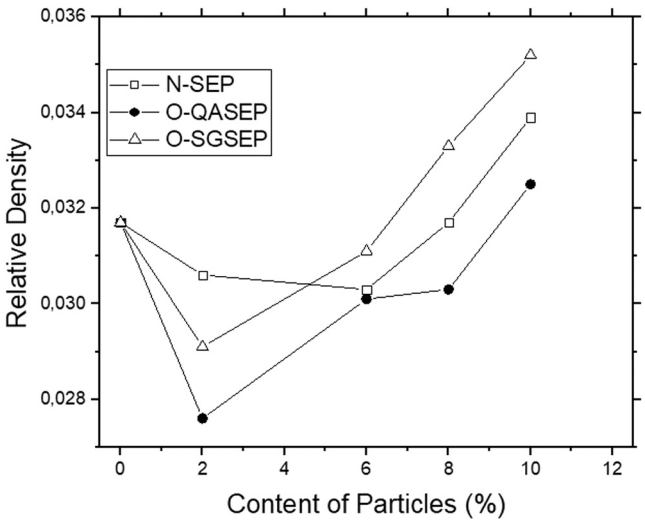

Fig. 5. Relative density vs the content of particles.

For instance, Yidong et al. incorporated attapulgite nanoparticles into a PS polymer and they detected an increase in the percentage of CO_2 absorbed by the material [60]. The reason behind this behavior could be that the presence of functional groups, like the hydroxyl groups (-OH) located in the surface of the sepiolites, could have a strong interaction with the CO_2 molecules [61]. Also, even when the particles were dried to remove moisture, some water could be still trapped in the clay, which could help to increase the absorption of the blowing agent [62].

However, when the particle content is higher than 8 wt% a decrease in the gas uptake is detected. One possible explanation for this change in the trend could be related to a change in the diffusivity when high contents of particles are introduced in the polymer matrix (that is, when the content of particles is close to the percolation threshold). If this occurs, as the gas uptake was measured at a fixed time (2 min) after releasing the pressure, it could happen that a significant amount of the CO_2 would have left the sample at the time of measurement.

The results also indicate that the composites containing O-QASEP present higher values of the gas uptake than the other materials. As it was previously shown these are the particles that better dispersed into the polymer matrix. This result could mean that when particles are agglomerated the chemical bonding interaction between the gas and the nanoparticles is less effective than when the particles are well dispersed. However, further studies would be required to check this hypothesis. In the composites, the amount of gas available for foaming is higher and this fact could have a significant effect on parameters like foam density, cell size, and cell nucleation density.

Fig. 5 shows the relationship between the relative density of the cellular materials and the content of sepiolites introduced in the system.

The behavior of the relative density is similar, independently of the type of particle considered. It is possible to see that the curve presents a minimum. It was expected that as soon as the percentage of particles increases the density of the material decreases since a higher amount of gas is introduced in the system (see Fig. 4). The relationship between the increase in the gas uptake and the reduction of the foam density has been reported before [63]. This trend is detected when working with contents of particles lower than 2 wt%. Moreover, it is also possible to see that there is a relationship between the gas uptake by each system and the foam density. For a content of particles of 2 wt% the sample containing N-SEP presents the lowest gas uptake and the highest density. On the contrary, the sample containing O-QASEP presents the highest gas uptake and the lowest density. However, an opposite trend is detected when adding higher content of particles. In this case, the density increases as the amount of particles increases. When the content of particles introduced increases the viscosity of the materials also suffers a

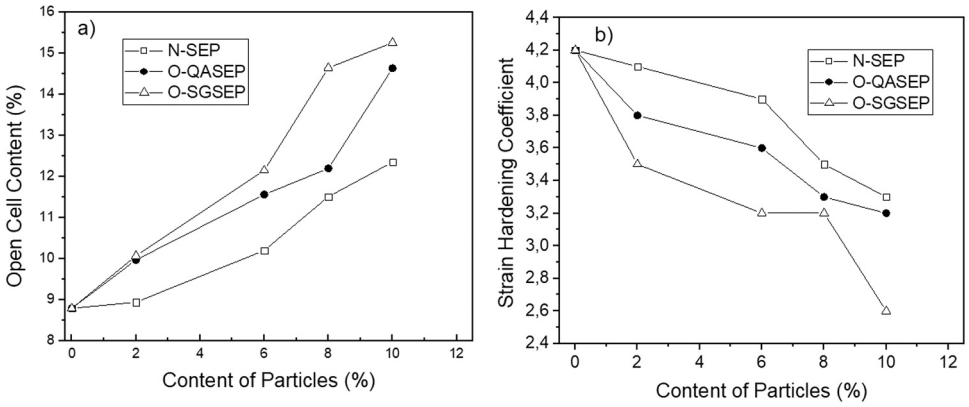

Fig. 6. (a) Open cell content as a function of the content of particles. (b) Strain hardening coefficient as a function of the content of particles.

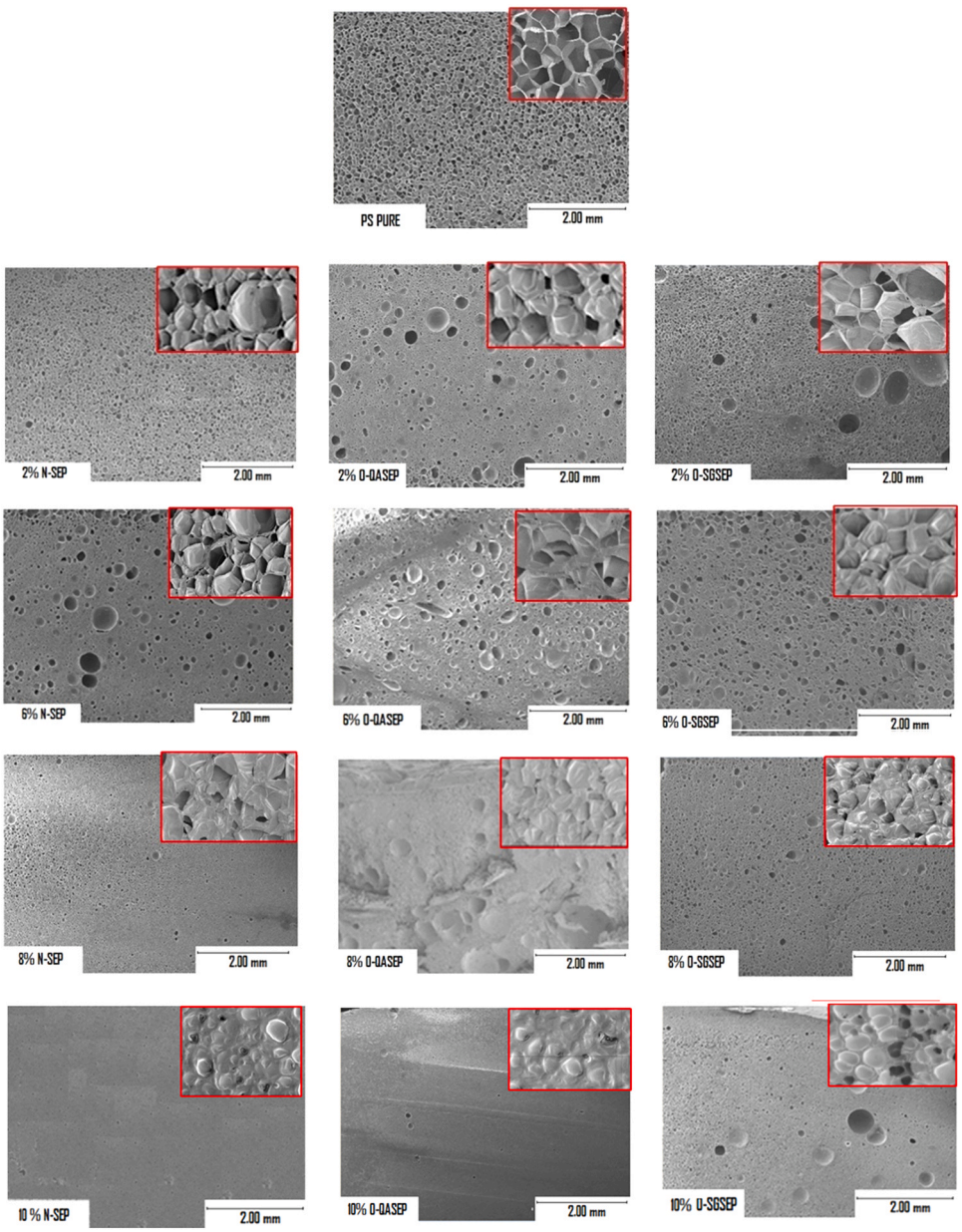

Fig. 7. SEM micrographs of the different foams. In a rectangle in the right upper side of each micrograph an image with a higher magnification is presented.

Table 4
Cell size, cell nucleation density, volumetric fraction of big cell and SD/φ of the cellular materials produced by the gas dissolution foaming process.

Sample Name	*Cell Size (μm)*	*Cell Nucleation Density (nuclei/cm^3)*	*Volumetric Fraction of Big Cells*	*SD/φ*
Pure PS	88.40 ± 28.12	(4.82 ± 0.52) x10^6	0	0.31
PS + 2% N-SEP	25.52 ± 3.88	(3.46 ± 0.34) x10^8	0.18	0.15
PS + 2% O-QASEP	15.92 ± 1.75	(3.82 ± 0.15) x10^8	0.15	0.10
PS + 2% O-SGSEP	30.30 ± 3.42	(3.33 ± 0.56) x10^8	0.22	0.11
PS + 6% N-SEP	19.14 ± 5.06	(3.73 ± 0.43) x10^8	0.21	0.26
PS + 6% O-QASEP	13.01 ± 2.69	(3.85 ± 0.12) x10^8	0.18	0.20
PS + 6% O-SGSEP	24.88 ± 4.65	(3.43 ± 0.70) x10^8	0.24	0.18
PS + 8% N-SEP	11.67 ± 2.93	(4.06 ± 0.36) x10^8	0.23	0.25
PS + 8% O-QASEP	9.22 ± 1.30	(4.15 ± 0.82) x10^8	0.21	0.14
PS + 8% O-SGSEP	17.14 ± 5.40	(3.75 ± 0.21) x10^8	0.26	0.31
PS + 10% N-SEP	12.97 ± 3.69	(4.02 ± 0.90) x10^8	0.26	0.28
PS + 10% O-QASEP	9.63 ± 1.36	(4.13 ± 1.07) x10^8	0.24	0.14
PS + 10% O-SGSEP	17.03 ± 4.02	(3.78 ± 0.11) x10^8	0.29	0.23

notorious increment. Consequently, the polymer finds the expansion more difficult despite having a higher concentration of gas. Therefore, the capability of the material to expand more thanks to the high content of the gas is playing against the increment of viscosity that sepiolites provide to the polymeric structure and therefore, a minimum is detected in the curve density vs. content of particles.

3.4. Open cell content

The open cell content of the different cellular materials has been also measured. The influence that this parameter has on the properties of the cellular materials has been widely studied. Generally, materials with high open cell contents exhibit poor mechanical properties, low thermal insulation capability, and improved acoustic absorption capacity [64,65]. Fig. 6(a) shows the open cell content values as a function of the percentage of particles. Additionally, Fig. 6(b) presents the strain hardening coefficient as a function of the content of particles.

Results show that all the foamed samples present a low value of the open cell content, varying between 9% and 15%. From Fig. 6(a) it can be concluded that the open cell content increases when the percentage of particles increases. Moreover, the same behavior occurs for the three types of particles. Results depicted in Fig. 6(b) indicates that when the content of particles increases the strain hardening coefficient is reduced. When a low-density cellular material is produced, the polymer contained in the cell walls is subjected to high extensional forces. If the polymer is not able to resist the extension, the thin cell walls break leading to an increase of the open cell content. In other words, the materials with a high strain hardening, that is, those containing low contents of particles, can resist the elongational forces occurring during the foaming process without breaking. As a result, the foams produced from these materials present low open cell contents. The decrease of the strain hardening (and therefore, the increase in the open cell content) detected when the amount of particles increases has been analyzed by several authors [39].

Fig. 6(a) also indicates that the foams containing N-SEP present the lowest values of the open cell content. By the contrary, the samples containing O-SGSE present the highest values of this parameter. This result could be explained considering, once again, Fig. 6(b), in which it is possible to see that the formulations containing N-SEP present the highest values of the strain hardening coefficient while the formulations containing O-SGSEP present the lowest values of this parameter. Therefore, there is a close relationship between the strain hardening behavior of the different formulations and the open cell content of the foamed materials.

3.5. Cellular structure

SEM micrographs of the cellular materials produced with the pure PS and with the different composites are depicted in Fig. 7. Several conclusions can be extracted from the qualitative observation of these images. On the one hand, the pure polymer displays a monomodal cellular structure. However, when sepiolites are introduced in the PS matrix, a bi-modal behavior is promoted. As it can be seen in Table 4 the volume fraction of large cells represents near 20% of the material. The large agglomerates of particles make possible the appearance of these large cells. The foams produced with the composites containing O-QASEP, which were the particles with the highest dispersion capability, present the lowest volumetric fraction of large cells. By the contrary, the foams produced with N-SEP and O-SGSEP, with a poor dispersion capability, show the highest volumetric fraction of big cells. Furthermore, the volume fraction of the large cells increases as the content of sepiolites increases. Nevertheless, apart from creating a bimodal structure, the sepiolites also play an essential role in the nucleation mechanisms. The foams produced with the sepiolite-based present cellular structures with lower cell sizes than those produced with pure PS.

From previous sections, it was extracted that the best dispersion degree was achieved with the O-QASEP. This result has an important effect on the cellular structure. Several works have demonstrated that the cell nucleation density strongly depends on the dispersion degree of the particles [39,66]. Moreover, higher cell nucleation densities are

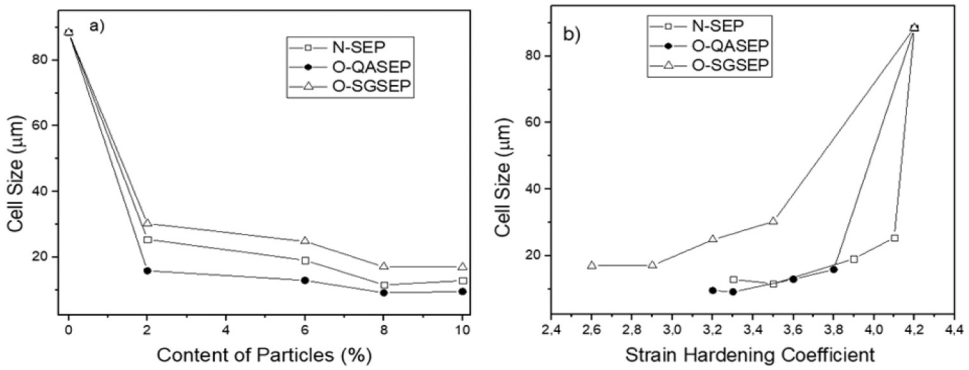

Fig. 8. (a) Correlation between the cell size and the content of particles. (b) Cell size of the cellular materials as a function of the strain hardening coefficient.

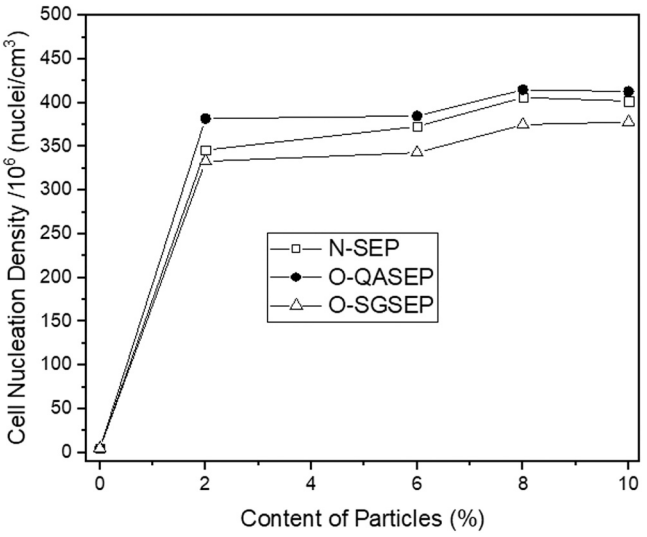

Fig. 9. Correlation between the content of particles introduced in the system and the cell nucleation density.

obtained with the polymeric systems that present an efficient dispersion. Nonetheless, extensional rheological parameters, like the strain hardening coefficient, are also critical to control the cell degeneration mechanisms by coalescence [39]. Therefore, both parameters, the dispersion degree and the strain hardening coefficient could have a critical effect on the cellular structure characteristics. Taking these ideas into account, several parameters accounting for the cellular structure such as cell size, the cell nucleation density and cell size distribution (SD/φ) have been analyzed in detail (see Table 4).

Results depicted in Table 4 and in Fig. 8(a) indicates that the cell size decreases when the percentage of particles increases. It is possible to obtain reductions in the cell size of 85%, 89% and 80%, with respect to the pure PS, when using 10 wt% of N-SEP, O-QASEP and O-SGSEP, respectively. That is, the foams with the lowest values of cell size are those containing O-QASEP while the foams with the highest values of the cell size are those containing O-SGSEP. These results indicate that in these polymeric systems there is a strong influence of the dispersion degree on the nucleation mechanisms and hence, in the cell size. The formulations presenting the higher dispersion degrees are those who lead to foams with the lowest cell sizes while the formulations presenting the lowest dispersion degrees are those who lead to foams with the highest cell sizes. Moreover, in Fig. 8(b) the relationship between the cell size and the strain hardening coefficient is represented. The cell size increases when the strain hardening coefficient increases. If the main factor controlling the cellular structure was the extensional rheological behavior of the formulations, as soon as the strain hardening coefficient increases, the cell size of the materials should decrease. However, in this case, is the other way around. This fact constitutes another proof that, in these systems, the nucleation mechanisms are the key factor controlling the cellular structure. These results demonstrate that, in these PS/sepiolites systems, the dispersion of particles is crucial to reach homogeneous cellular structures with low values of the cell size and high cell nucleation densities.

Cell nucleation density follows a similar trend than the cell size (see Fig. 9). As soon as sepiolites are introduced in the system an abrupt increase of the cell nucleation density is produced. Moreover, the cell nucleation density increases as the content of particles increases. Independently on the content of particles, the composite containing O-QASEP exhibits the highest cell nucleation density.

Finally, the homogeneity of the cellular structures is gathered in the SD/Φ parameter. Results included in Table 4 show that as soon as low percentages of sepiolites (close to 2%) are introduced in the PS matrix the cell size distributions become more homogeneous. This is something that could be explained considering the capability of the sepiolites to act as nucleants leading to finer and more homogeneous cellular structures. However, when a large content of particles is introduced (close to 10%), it is possible to see an increase in the value of SD/Φ, which indicates that the cellular structure is not as homogeneous as that of the foams containing low amounts of particles. This could be indicating that if the amount of particles is very high, they trend to agglomerate and as a consequence, the obtained cellular structure is more heterogeneous.

4. Conclusions

Blends of PS with different contents of sepiolites (2, 6, 8 and 10 wt%) both non-treated (N-SEP) and superficially treated with quaternary ammonium salts (O-QASEP) and with silane groups (O-SGSEP) have been prepared and foamed by gas dissolution foaming using CO_2 as blowing agent. The extensional rheological properties of the solid (non-foamed) composites have been analyzed as well as the dispersion degree of the particles in the PS matrix with the objective to analyze how the characteristics of the cellular structure are affected by these two parameters.

Extensional rheology results demonstrate that the strain hardening decreases as the clay content increases. Moreover, the composites produced with N-SEP presents the highest values of the strain hardening, while the lowest values are detected in the composites produced with the O-QASEP. A relationship between the strain hardening and the open cell content has been detected. The samples presenting the lowest values of the open cell content are those presenting the highest values of the strain hardening. In all the systems, the open cell content is always lower than 15%.

The dispersion degree of the particles in the PS matrix has been characterized by shear rheology. The obtained results indicate that O-QASEP present a much better dispersion degree than the other two particles. The way in which the particles are dispersed in the PS matrix has an important effect on the cellular structure. The highest reductions in the cell size, with respect to the foams produced with the virgin PP, are detected in the foams produced with the composites containing O-QASEP. A reduction of the cell size of approximately 90% and an increase in the cell nucleation density of around 90 times is obtained when adding 8 wt% of O-QASEP.

From these results, it is possible to conclude that in these polymeric systems the degeneration mechanisms, which are conditioned by the extensional rheological behavior of the polymer matrix, are more intensive in the samples containing clays and they have an important effect in the open cell content. However, nucleation mechanisms, which in turn mainly depend on how the particles are dispersed in the PS matrix, are the key factor controlling the cellular structure (cell size, cell homogeneity and cell nucleation density). Therefore, in these systems to obtain a reduction in the cell size it is necessary to start from a formulation in which the particles are perfectly dispersed in the polymer matrix without forming agglomerates.

CRediT authorship contribution statement

A. Ballesteros: Investigation, Writing – original draft. **E. Laguna-Gutierrez:** Writing – review & editing, Resources. **M.L. Puertas**: Resources, Project administration. **A. Esteban-Cubillo**: Resources, Project administration. **J. Santaren:** Resources, Project administration. **M.A. Rodriguez-Perez:** Conceptualization, Writing – review & editing, Supervision.

Declaration of Competing Interest

The authors declare that they have no known competing financial interests or personal relationships that could have appeared to influence the work reported in this paper.

Acknowledgments

Financial assistance from the Junta of Castile and Leon (VA202P20) and Spanish Ministry of Science, Innovation and Universities (RTI2018-098749-B-I00) and the "Ente Público Regional de la Energía de Castilla y León" (EREN) are gratefully acknowledged.

Appendix A. Supporting information

Supplementary data associated with this article can be found in the online version at doi:10.1016/j.mtcomm.2021.102850.

References

[1] A.K. Kota, B.H. Cipriano, M.K. Duesterberg, Electrical and rheological percolation in polystyrene/MWCNT nanocomposites, Macromolecules 40 (20) (2007) 7400–7406, https://doi.org/10.1021/ma0711792.
[2] V. Dolomanova, J.C.M. Rauhe, L.R. Jensen, R. Pyrz, A.B. Timmons, Mechanical properties and morphology of nano-reinforced rigid PU foam, J. Cell Plast. 47 (1) (2011) 81–93, https://doi.org/10.1177/0021955×10392200.
[3] H. Mauroy, T.S. Plivelic, J.P. Suuronen, F.S. Hage, J.O. Fossum, K.D. Knudsen, Anisotropic clay–polystyrene nanocomposites: synthesis, characterization and mechanical properties, Appl. Clay Sci. 108 (2015) 19–27, https://doi.org/10.1016/J.CLAY.2015.01.034.
[4] L.J. Lee, C. Zeng, X. Cao, X. Han, J. Shen, G. Xu, Polymer nanocomposite foams, Compos Sci. Technol. 65 (15–16 SPEC. ISS.) (2005) 2344–2363, https://doi.org/10.1016/j.compscitech.2005.06.016.
[5] M. Santiago-Calvo, J. Tirado-Mediavilla, J.C. Rauhe, L.R. Jensen, J.L. Ruiz-Herrero, F. Villafañez, M.A. Rodriguez-Perez, Evaluation of the thermal conductivity and mechanical properties of water blown polyurethane rigid foams reinforced with carbon nanofibers, Eur. Polym. J. 108 (2018) 98–106, https://doi.org/10.1016/j.eurpolymj.2018.08.051.
[6] J.U. Park, J.L. Kim, D.H. Kim, K.H. Ahn, S.J. Lee, K.S. Cho, Rheological behavior of polymer/layered silicate nanocomposites under uniaxial extensional flow, Macromol. Res. 14 (3) (2006) 318–323, https://doi.org/10.1007/BF03219088.
[7] S. Doroudiani, M.T. Kortschot, Polystyrene foams: II. Structure-impact properties relationships, J. Appl. Polym. Sci. 90 (5) (2003) 1421–1426, https://doi.org/10.1002/app.12805.
[8] M. Okamoto, P.H. Nam, P. Maiti, T. Kotaka, Hasegawa Naoki, A. Usuki, A house of cards structure in polypropylene/clay nanocomposites under elongational flow, Nano Lett. 1 (2001) 295–298, https://doi.org/10.1021/NL0100163.
[9] C.C. Ibeh, Thermoplastic materials: properties, manufacturing methods, and applications.
[10] https://www.thecowboychannel.com/story/43663399/polystyrene-market-2021-is-estimated-to-clock-a-modest-cagr-of-26nbspduring-the-forecast-period-2021-2026-with-top-countries-data. 2021.
[11] Y. Chen, R. Das, M. Battley, Effects of cell size and cell wall thickness variations on the stiffness of closed-cell foams, Int. J. Solids Struct. 52 (2015) (2005) 150–164, https://doi.org/10.1016/J.IJSOLSTR.2014.09.022.
[12] C. Zhang, B. Zhu, L.J. Lee, Extrusion foaming of polystyrene/carbon particles using carbon dioxide and water as co-blowing agents, Polymer 52 (2011) (2011) 1847–1855.
[13] X. Han, C. Zeng, L.J. Lee, K.W. Koelling, D.L. Tomasko, Extrusion of polystyrene nanocomposite foams with supercritical CO_2, Polym. Eng. Sci. 43 (6) (2003) 1261–1275, https://doi.org/10.1002/pen.10107.
[14] Y. Fei, W. Fang, Z. Mingqiang, J. Jiangming, Extrusion foaming of lightweight polystyrene composite foams with controllable cellular structure for sound absorption application, Polymer 11 (2019) 106, https://doi.org/10.3390/polym11010106.
[15] J. Shen, X. Han, L.J. Lee, Nanoscaled reinforcement of polystyrene foams using carbon nanofibers, J. Cell. Plast. 42 (2006) 105–126, https://doi.org/10.1177/0021955×06060947.
[16] S. Bourbigot, J.W. Gilman, C.A. Wilkie, Kinetic analysis of the thermal degradation of polystyrene–montmorillonite nanocomposite, Polym. Degrad. Stab. 84 (3) (2004) 483–492, https://doi.org/10.1016/J.Polymdegradstab.2004.01.006.
[17] E. Kontou, G. Anthoulis, The effect of silica nanoparticles on the thermomechanical properties of polystyrene, J. Appl. Polym. Sci. 105 (4) (2007) 1723–1731, https://doi.org/10.1002/app.26409.
[18] J. Yang, L. Huang, Y. Zhang, F. Chen, M. Zhong, Mesoporous silica particles grafted with polystyrene brushes as a nucleation agent for polystyrene supercritical carbon dioxide foaming, J. Appl. Polym. Sci. 130 (6) (2013) 4308–4317, https://doi.org/10.1002/app.39532.
[19] V. Bernardo, J. Martin-de Leon, E. Laguna-Gutierrez, M.A. Rodriguez-Perez, PMMA-sepiolite nanocomposites as new promising materials for the production of nanocellular polymers, Eur. Polym. J. 96 (2017) 10–26, https://doi.org/10.1016/j.eurpolymj.2017.09.002.
[20] M.S. Nikolic, R. Petrovic, D. Veljovic, V. Cosovic, N. Stankovic, J. Djonlagic, Effect of sepiolite organomodification on the performance of PCL/sepiolite nanocomposites, Eur. Polym. J. 97 (October) (2017) 198–209, https://doi.org/10.1016/j.eurpolymj.2017.10.010.
[21] P. Lu, The effects of different grafted clays on thermal properties of their PMMA composites, Polym. Plast. Technol. Eng. 50 (15) (2011) 1541–1545, https://doi.org/10.1080/03602559.2011.603780.
[22] M. Alexandre, P. Dubois, Polymer-layered silicate nanocomposites: preparation, properties and uses of a new class of materials, Mater. Sci. Eng. R. Rep. 28 (1–2) (2000) 1–63, https://doi.org/10.1016/S0927-796X(00)00012-7.
[23] N.A. Mohd Zaini, H. Ismail, A. Rusli, Short review on sepiolite-filled polymer nanocomposites, Polym. Plast. Technol. Eng. 56 (15) (2017) 1665–1679, https://doi.org/10.1080/03602559.2017.1289395.
[24] V. Bernardo, J. Martin-de Leon, M.A. Rodriguez-Perez, Anisotropy in nanocellular polymers promoted by the addition of needle-like sepiolites, Polym. Int. 68 (2019) 1204–1214, https://doi.org/10.1002/pi.5813.
[25] Notario B. , Velasco D. , Esteban-Cubillo A. , Santarén J. , Rodriguez-Perez M.A. Improving the cellular structure and thermal conductivity of polysyrene foams by using sepiolites. in International Conference on Foams,Foams Technology, FOAMS 2012, 1–5 (2012).
[26] J. Zhang, S. de Juan, A. Esteban-Cubillo, J. Santarén, D.Y. Wang, Effect of organo-modified nanosepiolite on fire behaviors and mechanical performance of polypropylene composites, Chin. J. Chem. 33 (2) (2015) 285–291, https://doi.org/10.1002/cjoc.201400828.
[27] N.H. Huang, Z.J. Chen, J.Q. Wang, P. Wei, Synergistic effects of sepiolite on intumescent flame retardant polypropylene, Express Polym. Lett. 4 (12) (2010) 743–752, https://doi.org/10.3144/expresspolymlett.2010.90.
[28] D. Killeen, M. Frydrych, B. Chen, Porous poly(vinyl alcohol)/sepiolite bone scaffolds: preparation, structure and mechanical properties, Mater. Sci. Eng. C 32 (4) (2012) 749–757, https://doi.org/10.1016/j.msec.2012.01.019.
[29] Y. Zheng, Y. Zheng, Study on sepiolite-reinforced polymeric nanocomposites, J. Appl. Polym. Sci. 99 (5) (2006) 2163–2166, https://doi.org/10.1002/app.22337.
[30] M. Liu, M. Pu, H. Ma, Preparation, structure and thermal properties of polylactide/sepiolite nanocomposites with and without organic modifiers, Compos Sci. Technol. 72 (13) (2012) 1508–1514, https://doi.org/10.1016/J.COMPSCITECH.2012.05.017.
[31] S. Xie, S. Zhang, F. Wang, M. Yang, R. Seguela, J.M. Lefebvre, Preparation, structure and thermomechanical properties of nylon-6 nanocomposites with lamella-type and fiber-type sepiolite, Compos Sci. Technol. 67 (11–12) (2007) 2334–2341, https://doi.org/10.1016/J.COMPSCITECH.2007.01.012.
[32] D. Garcia-Lopez, J.F. Fernandez, J.C. Merino, J. Santaren, J.M. Pastor, Effect of organic modification of sepiolite for PA 6 polymer/organoclay nanocomposites, Compos Sci. Technol. 70 (10) (2010) 1429–1436, https://doi.org/10.1016/j.compscitech.2010.05.020.
[33] G.J. Nam, J.H. Yoo, J.W. Lee, Effect of long-chain branches of polypropylene on rheological properties and foam-extrusion performances, J. Appl. Polym. Sci. 96 (2005) 1793–1800, https://doi.org/10.1002/app.21619.
[34] H.G.H. Van Melick, L.E. Govaert, H.E.H. Meijer, On the origin of strain hardening in glassy polymers, Polymer 44 (2003) 2493–2502, https://doi.org/10.1016/S0032-3861(03)00112-5.
[35] P.M. Wood-Adams, J.M. Dealy, Using rheological data to determine the branching level in metallocene polyethylenes, Macromolecules 33 (20) (2000) 7481–7488, https://doi.org/10.1021/ma991534r.
[36] U. ParkJ, L.K. Jeong, D.H. Kim, K.H. Ahn, S.J. Lee, K.S. Cho, Rheological behavior of polymer/layered silicate nanocomposites under uniaxial extensional flow, Macromol. Res. 14 (2006) 318–323, https://doi.org/10.1007/BF03219088.
[37] B.A. Morris, Rheology of Polymer Melts. The Science and Technology of Flexible Packaging, Elsevier, 2017, pp. 121–147, https://doi.org/10.1016/B978-0-323-24273-8.00005-8.
[38] K. Taki, K. Tabata, S. Kihara, M. Ohshima, Bubble coalescence in foaming process of polymers, Polym. Eng. Sci. 46 (2006) 680–690, https://doi.org/10.1002/pen.20521.
[39] E. Laguna-Gutierrez, A. Lopez-Gil, C. Saiz-Arroyo, R. Van Hooghteen, P. Moldenaers, M.A. Rodriguez-Perez, Extensional rheology, cellular structure, mechanical behavior relationships in HMS PP/montmorillonite foams with similar densities, J. Polym. Res. 23 (2016) 251, https://doi.org/10.1007/s10965-016-1143-x.
[40] M. Kobayashi, T. Takahashi, J. Takimot, K. Koyama, Flow-induced whisker orientation and viscosity for molten composite systems in a uniaxial elongational flow field, Polymer 36 (1995) 3927–3933, https://doi.org/10.1016/0032-3861(95)99787-U.
[41] M. Koki, D.K. Christopher, W.K. Kurt, M. Monon, E.B. Stephen, Shear and extensional rheology and flow-induced orientation of carbon nanofiber/polystyrene melt composites, J. Appl. Polym. Sci. 119 (2011) 1940–1951.
[42] R. Kotsilkova, Rheology–structure relationship of polymer/layered silicate hybrids, Mech. Time Depend. Mater. 6 (2002) 283–300.
[43] R.K. Gupta, V. Pasanovic-Zujo, S.N. Bhattacharya, Shear and extensional rheology of EVA/layered silicate-nanocomposites, J. Nonnewton. Fluid Mech. 128 (2005) 116–125.
[44] L.A. Utracki, P. Sammut, On the uniaxial extensional flow of polystyrene/polyethylene blends, Polym. Eng. Sci. 30 (1990) 1019–1026.
[45] T. Takahashi, W. Wu, H. Toda, J.I. Takimoto, T. Akatsuka, K. Koayama, Elongational viscosity of ABS polymer melts with soft or hard butadiene particles, J. Nonnewton. Fluid Mech. 68 (1997) 259–269.
[46] M. Kobayashi, T. Takahashi, J.I. Takimoto, K. Koyama, Influence of glass beads on the elongational viscosity of polyethylene with anomalous strain rate dependence of the strain-hardening, Polym. (Guildf.) 37 (1996) 3745–3747.

[47] J.F. Le Meins, P. Moldenaers, J. Mewis, Suspensions of monodisperse spheres in polymer melts: particle size effects in extensional flow, Rheol. Acta 42 (2003) 184–190.
[48] V.I. Kalikmanov, Nucleation Theory, Springer, 2013.
[49] Y.H. Lee, C.B. Park, K.H. Wang, M.H. Lee, HDPE-Clay nanocomposite foams blown with supercritical CO_2, J. Cell. Plast. 41 (2005) 487–502.
[50] J.A. De Lima, F.F. Camilo, R. Faez, S.A. Cruz, A new approch to sepiolite dispersion by treatment with ionic liquids, Appl. Clay Sci. 143 (2017) 234–240.
[51] J. Sandler, M.S.P. Shaffer, T. Prasse, W. Bauhofer, K. Schulte, A.H. Windle, Development of a dispersion process for carbon nanotubes in an epoxy matrix and the resulting electrical properties, Polymer 40 (1999) 5967–5971.
[52] E. Bilotti, H.R. Fischer, T. Peijs, Polymer nanocomposites based on needle-like sepiolite clays: effect of functionalized polymers on the dispersion of nanofiller, crystallinity, and mechanical properties, J. Appl. Polym. Sci. 107 (2007) 1116–1123.
[53] N. García, J. Guzman, E. Benito, A. Esteban-Cubillo, E. Aguilar, J. Santaren, P. Tiemblo, Surface modification of sepiolite in aqueous gels by using methoxysilanes and its impact on the nanofiber dispersion ability, Langmuir 27 (2011) 3952–3959.
[54] S.K. Goel, E.J. Beckman, Generation of microcellular polymers using supercritical carbon dioxide I: effect of pressure and temperature on nucleation, Polym. Eng. Sci. 34 (1993) 1137–1147.
[55] V. Kumar, P. Nam, A. Shu, A process for making microcellular thermoplastic parts, Polym. Eng. Sci. 30 (1990) 1323–1329.
[56] Münstedt H. , Schwarzl F.R. Deformation and flow of polymeric materials.
[57] J. Pinto, E. Solorzano, M.A. Rodriguez-Perez, J.A. De Saja, Erratum for PMID 21180585, Ther. Adv. Gastroenterol. 5 (2012) 371, https://doi.org/10.1177/0021955×13503847.
[58] E. Laguna-Gutierrez, R. Van Hooghten, P. Moldenaers, M.A. Rodriguez-Perez, Effects of extrusion process, type and content of clays, and foaming process on the clay exfoliation in HMS PP composites, J. Appl. Polym. Sci. 132 (2015) 1–12.
[59] J. Zhao, A.B. Morgan, J.D. Harris, Rheological characterization of polystyrene-clay nanocomposites to compare the degree of exfoliation and dispersion, Polymer 46 (2005) 8641–8660.
[60] Y. Liu, L. Jian, T. Xiao, R. Liu, S. Yi, S. Zhang, L. Wang, R. Wang, Y. Min, High performance attapulgite/polypyrrole nanocomposite reinforced polystyrene (PS) foam based on supercritical CO_2 foaming, Polymers 11 (2019) 985.
[61] H. Wan, Y. Que, C. Chen, Z. Wu, Preparation of metal-organic framework/attapulgite hybrid material for CO 2 capture, Mater. Lett. 194 (2017) 107–109.
[62] N.H. Abu-Zahra, A.M. Alian, Density and cell morphology of rigid foam PVC-Clay nanocomposites, Polym. Plast. Technol. Eng. 49 (2010) 237–243.
[63] E. Di Maio, G. Mensitieri, S. Iannace, L. Nicolais, W. Li, R.W. Flumerfelt, Structure optimization of polycaprolactone foams by using mixtures of CO_2 and N2 as blowing agents, Polym. Eng. Sci. 45 (2005) 432–441.
[64] M. Alvarez-Lainez, M.A. Rodríguez-Perez, J.A. De Saja, Thermal conductivity of open-cell polyolefin foams, J. Polym. Sci. Part B Polym. Phys. 46 (2008) 212–221.
[65] M.A. Rodriguez-Perez, M. Alvarez-Lainez, J.A. De Saja, Microstructure and physical properties of open-cell polyolefin foams, Appl. Polym. Sci. 114 (2009) 1176–1186.
[66] E. Solórzano, M.A. Rodriguez-Perez, J. Lazaro, J.A. De Saja, Influence of solid phase conductivity and cellular structure on the heat transfer mechanisms of cellular materials: diverse case studies, Adv. Eng. Mater. 11 (2009) 818–824.